# Novel Soft Chemical Method for Optically Transparent $Ru(bpy)_3$-$K_4Nb_6O_{17}$ Thin Film

**Zhiwei Tong,[†] Shinsuke Takagi,[†] Hiroshi Tachibana,[†] Katsuhiko Takagi,[‡] and Haruo Inoue*[,†,§]**

*Department of Applied Chemistry, Graduate Course of Engineering, Tokyo Metropolitan University, 1-1 Minami-ohsawa, Hachiohji-city, Tokyo 192-0397, Japan, Department of Crystalline Materials Science, Graduate School of Engineering, Nagoya University, Furocho, Chikusaku, Nagoya 464-8603, Japan, CREST (Japan Science and Technology), Japan*

*Received: August 23, 2005; In Final Form: September 21, 2005*

A unique guest−guest ion exchange method was developed for preparing a thin film of a nano-layered $K_4Nb_6O_{17}\cdot 3H_2O$ that possesses both (1) optical transparency and (2) ion-exchangeability under ambient conditions without calcination at high temperature. An optically transparent $Ru(bpy)_3^{2+}$-$K_4Nb_6O_{17}$ hybrid thin film, a photoresponsive electrode, was successfully prepared by the guest−guest exchange method by use of the intercalation compound $MV^{2+}$-$K_4Nb_6O_{17}$ as a precursor. The optically transparent $Ru(bpy)_3^{2+}$-$K_4Nb_6O_{17}$ hybrid thin films have been characterized by X-ray diffraction, SEM, AFM, IR, and UV spectroscopies, as well as elemental analysis. The electrochemical behavior of the ITO/$Ru(bpy)_3^{2+}$-$K_4Nb_6O_{17}$ hybrid thin film electrode was studied; it also exhibits swift photoresponse in the visible region.

## Introduction

The nanolayer-structured semiconductor potassium niobates ($K_4Nb_6O_{17}\cdot 3H_2O$) have attracted considerable attention due to their unique structural properties[1] and application in various aspects such as intercalation reactions,[2−4] photocatalysis,[5−7] electrochemical activity,[8] and ionic exchange processes.[9,10] There are also many reports on new composite materials which originate from various layered compounds.[11] Although many of these layered materials have been prepared in the form of thin films, it is very rare that the material retains its ion-exchange capability.[12] Most layered materials lose their ion-exchangeability when they are in the form of thin films. If films having ion-exchange capability could be obtained, various useful materials with many potential applications could be prepared.

Photoprocesses on solid surfaces have attracted increasing attention from the viewpoint of various applications such as solar energy conversion and photoresponsive thin films.[13] Recent reports on the efficient sensitization of semiconductor nanocrystallites with inorganic[14−17] and organic[18−24] dyes have stimulated much interest in developing nanostructured semiconductor films as photoresponsive electrode materials for photoelectrochemical cells.[25−27] Among various subjects to be solved, optical transparency is one of the most preferred requisites for these applications. Most materials, however, only serve as optically nontransparent thin films. The methodology of how to prepare transparent thin films under the ambient conditions should be one of the most crucial key technologies in this field.

Several reports on intercalation of the photosensitizer, $Ru(bpy)_3^{2+}$, into the niobate layer have appeared.[3,28−31] Domen et al. reported a femtosecond transient spectroscopy of the $Ru(bpy)_3^{2+}$ intercalated niobate and observed an electron injection from the excited $Ru(bpy)_3^{2+}$ to the conduction band of niobate.[30] The film prepararion, however, still required a high-temperature calciantion at 1073 K and $Ru(bpy)_3^{2+}$ was intercalated into both layers I and II of niobate.[31] The more convenient and the milder conditions should be requisite for the more developed application. In this paper we report a unique guest−guest ion exchange method for preparing a thin film of a nanolayered $K_4Nb_6O_{17}\cdot 3H_2O$ that possesses both (1) the optical transparency and (2) ion-exchangeability under ambient conditions without calcianation procedures at high temperature. Tris(2,2′-bipyridine)-ruthenium(II) complex ($Ru(bpy)_3^{2+}$) as a photosensitizer was successfully and selectively intercalated into only layer I of the optically transparent nanolayered niobate. The optical transparency of the film was excellent as shown later (Figure 4).

## Experimental Section

The layered compound, $K_4Nb_6O_{17}\cdot 3H_2O$, employed here was prepared by calcination of a 2.1:3.0 molar mixture of $K_2CO_3$ and $Nb_2O_5$ at 1100 °C for 10 h, according to the procedures reported by Nassau et al.[32] Methyl viologen chloride was purchased from Tokyo Kasei; $Ru(bpy)_3Cl_2\cdot 6H_2O$ was purchased from Aldrich and used without further purification.

Figure 1 shows the layered structure of $K_4Nb_6O_{17}\cdot 3H_2O$. $K_4Nb_6O_{17}$ consists of octahedral units of $NbO_6$, which form a two-dimensional layered structure via bridging oxygen atoms. The layers are negatively charged, and $K^+$ ions exist between the layers to compensate for the negative charges of the layers.[1] The intercalation compounds of $K_4Nb_6O_{17}$ with $Ru(bpy)_3^{2+}$ are generally very difficult to prepare by a direct reaction because of the bulkiness of $Ru(bpy)_3^{2+}$.[28] A two-step intercalation was thus attempted by adopting methyl viologen-$K_4Nb_6O_{17}$ intercalation compounds as the intermediates. The methyl viologen ($MV^{2+}$) can be smoothly intercalated into interlayer I of $K_4Nb_6O_{17}$,[33,34] since interlayer I is more labile than interlayer II. The intercalation of $MV^{2+}$ ions into $K_4Nb_6O_{17}$ was carried out by treating $K_4Nb_6O_{17}\cdot 3H_2O$ with an aqueous solution of excess methyl viologen chloride and then allowing it to stand for 3 weeks at 70 °C. The resultant product was washed with deionized water until the $MV^{2+}$ absorption could not be detected

* Address correspondence to this author. E-mail: inoue-haruo@c.metro-u.ac.jp.
[†] Tokyo Metropolitan University.
[‡] Nagoya University.
[§] CREST.

10.1021/jp054742w CCC: $30.25 
Published on Web 10/21/2005

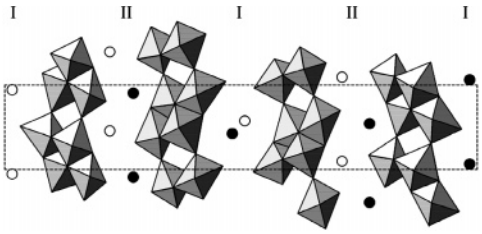


**Figure 1.** The structure of $K_4Nb_6O_{17}$·$3H_2O$ showing the two interlayer regions. Squares represent the $NbO_6$ octahedra, and the circles indicate the exchangeable cation $K^+$ within the interlayers.

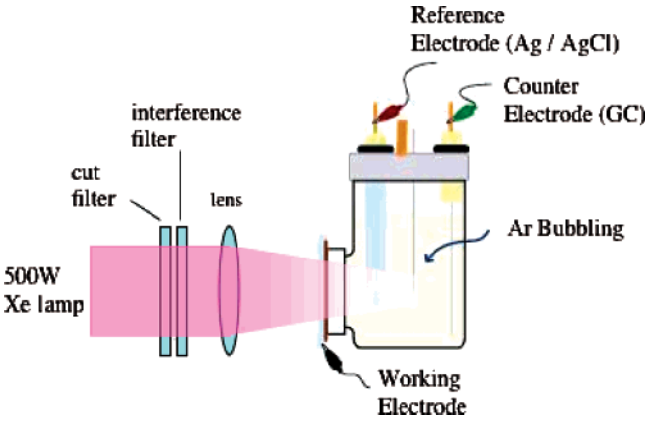


**Figure 2.** Schematic illustration of apparatus for spectroelectrochemical and photocurrent measurement.

at 257 nm in the filtrate solution. The second step in preparing the $Ru(bpy)_3^{2+}$-$K_4Nb_6O_{17}$ thin film electrode was as follows: A 200-$\mu$L aqueous suspension of the $MV^{2+}$-$K_4Nb_6O_{17}$ hybrid was coated onto an ITO (indium tin oxide) glass electrode. The sample was dried at 60 °C for 2 h in air. The area of the formed thin film electrode was about 2 $cm^2$. $Ru(bpy)_3^{2+}$ turned out to be readily intercalated via a guest−guest ion-exchange method into the interlayer of the $MV^{2+}$-$K_4Nb_6O_{17}$ hybrid thin film via placing the electrode in a 3mM $Ru(bpy)_3^{2+}$ aqueous solution for 4 days. The optically transparent $Ru(bpy)_3^{2+}$-$K_4Nb_6O_{17}$ hybrid thin film electrode was washed with deionized water until the $Ru(bpy)_3^{2+}$ absorption could not be detected at 452 nm in the filtrate solution. Characterizations of the optically transparent $Ru(bpy)_3^{2+}$-$K_4Nb_6O_{17}$ hybrid thin film were carried out by means of X-ray diffraction, SEM, AFM, IR, and UV spectroscopies, as well as elemental analysis. X-ray diffraction analysis was carried out with a M21X (MAC Co., Ltd.) diffractometer with monochromatic Cu K$\alpha$ radiation ($\lambda$ = 0.15406 nm) with 2$\theta$ going from 1.5° to 30° in 1° steps. SEM images were performed with a JSM6100 scanning electron microscope. AFM images were taken with a Seiko SPA 300 microscope operated in a noncontact mode. The infrared spectra were recorded on a JASCO FT-IR spectrometer with the use of KBr pellets. The UV spectra were measured with JASCO V-550 spectrophotometers. Elemental analysis (EA) data were obtained with a Perkin-Elmer 2400-CHN elemental analyzer.

The photoelectrochemical experiments of the optically transparent $Ru(bpy)_3^{2+}$-$K_4Nb_6O_{17}$ hybrid thin film electrode were performed in a three-electrode cell. Ag/AgCl and glassy carbon were used as the reference and counter electrodes, respectively. The photoelectrochemical cell employed in the present set of experiments is shown in Figure 2.

A potentiostat, HZ-3000 (Hokuto Denko), and a function generator, BS100 (Hokuto Denko), were used in electrochemical measurements. Photocurrent measurements were carried out with a Model HA-501 potentiostat and a GOULD DSO4072 digital storage oscilloscope (100M). A collimated light beam from a 500-W xenon lamp (USHIO 500-DKO) was used as the light source. A pair of cutoff filters (UV-39) and an interference filter (KL-43(430 nm), KL-44(440 nm), KL-45(450 nm), KL-46(460 nm), KL-47(470 nm), KL-48(480 nm), KL-49(490 nm), KL-51(510 nm), KL-52(520 nm), KL-53(530 nm), KL-55(550 nm), KL-56(560 nm)) were introduced into the path of the excitation beam to select the excitation wavelength. The intensity of the irradiated light was measured with an Advantest TQ8210 optical power meter.

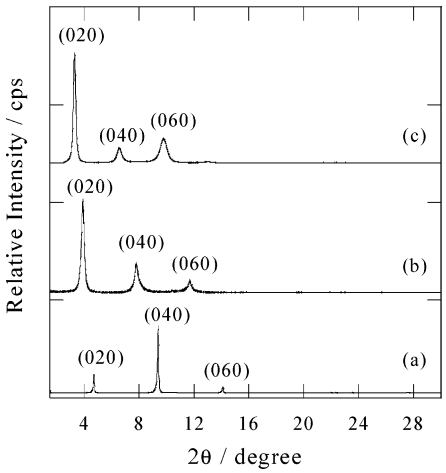


**Figure 3.** The X-ray diffraction patterns of (a) $K_4Nb_6O_{17}$·$3H_2O$, (b) $MV^{2+}$-$K_4Nb_6O_{17}$ thin film, and (c) $Ru(bpy)_3^{2+}$-$K_4Nb_6O_{17}$ thin film.

**TABLE 1: X-ray Diffraction Spectrum Data**

| compd | $d_{120}$/nm | $d_{040}$/nm | $\Delta d^a$/nm |
|---|---|---|---|
| $K_4Nb_6O_{17}$·$3H_2O$ | 1.88 | 0.94 | |
| $K_4Nb_6O_{17}$ | (1.64) | 0.82 | |
| $MV^{2+}$-$K_4Nb_6O_{17}$ | 2.26 | 1.13 | 0.62 |
| $Ru(bpy)_3^{2+}$-$K_4Nb_6O_{17}$ | 2.72 | 1.36 | 1.08 |

[a] $\Delta d$ means the increase in $d_{020}$ from that of $K_4Nb_6O_{17}$ (2 × $d_{040}$ = 1.64 nm).

## Results and Discussion

**Characterization of the $Ru(bpy)_3^{2+}$-$K_4Nb_6O_{17}$ Thin Film.** The layered compound, $K_4Nb_6O_{17}$·$3H_2O$, was identified by powder X-ray diffraction analysis (Figure 3a).[32] The hydrated potassium niobate, $K_4Nb_6O_{17}$·$3H_2O$, exhibits a (020) diffraction peak at 1.88 nm accompanied by an intense (040) peak at 0.94 nm in its XRD pattern (Figure 3a, Table 1). The $d_{020}$ values, corresponding to the sum of two adjacent interlayer spacings, are regarded as the basal spacing; these adjacent two interlayers have microenvironments different from each other: water adsorbs only in interlayer I.[28]

The methyl viologen dication ($MV^{2+}$) is intercalated only into interlayer I.[34] The 2$\theta$ angle of the (020) diffraction peak of $MV^{2+}$-$K_4Nb_6O_{17}$ was smaller than that of the untreated $K_4Nb_6O_{17}$·$3H_2O$ (Figure 3b). The $d_{020}$ was expanded up to 2.26 nm ($\Delta d$ = 0.62 nm). The arrangement of the intercalated $MV^{2+}$ ions could be inferred from the $\Delta d$ values. It has been reported that the intercalation of a flat monolayer $MV^{2+}$ ion into layered materials gives $\Delta d$ values of 0.28∼0.33 nm.[35,36] Therefore, the $MV^{2+}$ ions were suggested to be intercalated with an inclined orientation versus the layer sheet of interlayer I of $K_4Nb_6O_{17}$·$3H_2O$. The introduction of $Ru(bpy)_3^{2+}$ into the layered niobate resulted in a ca. +1.08 nm shift in the basal spacing ($\Delta d$) compared with the anhydrous $K_4Nb_6O_{17}$ (Figure 3c and Table 1) by the guest−guest ion exchange method. The XRD patterns

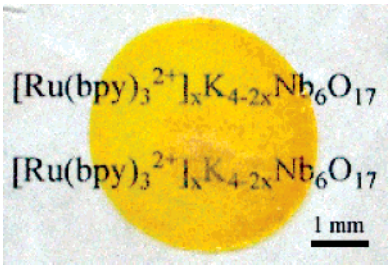


**Figure 4.** Photograph of the $Ru(bpy)_3^{2+}$-$K_4Nb_6O_{17}$ hybrid thin film. The yellow circle is the hybrid thin film. The letters are printed beneath the thin film and can be seen through the film.

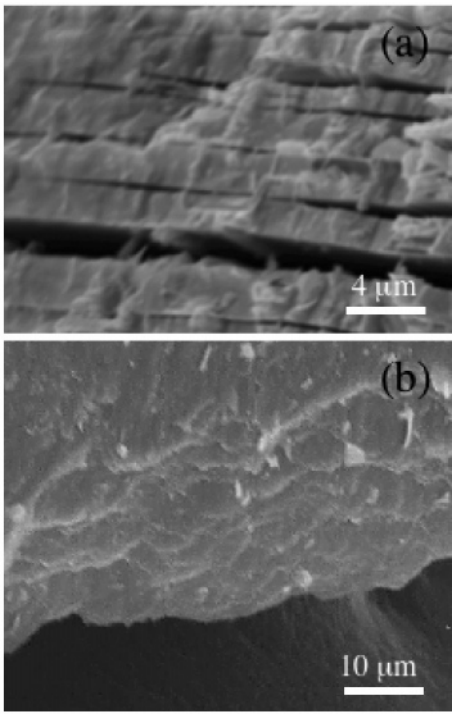


**Figure 5.** Scanning electron micrographs of (a) the $K_4Nb_6O_{17}$ crystal and (b) the $Ru(bpy)_3^{2+}$-$K_4Nb_6O_{17}$ thin film.

of $Ru(bpy)_3^{2+}$-$K_4Nb_6O_{17}$ as the reaction product maintained a diffraction pattern profile similar to that of the intermediate, $MV^{2+}$-$K_4Nb_6O_{17}$, even though the positions of the (0*k*0) peaks changed (Figure 3b,c). The basic structure of the intermediate was, thus, concluded to be retained in the intercalation compounds, $Ru(bpy)_3^{2+}$-$K_4Nb_6O_{17}$, i.e., with $Ru(bpy)_3^{2+}$ situated in interlayer I only. A photograph of an optically transparent $Ru(bpy)_3^{2+}$-$K_4Nb_6O_{17}$ hybrid thin film is shown in Figure 4. The film exhibited excellent transparency in the visible region.

The thin film has a thickness of about 15 $\mu$m, as directly estimated by SEM, shown in Figure 5; two-dimensional niobate sheets parallel to the glass plate are observed. The optical transparency is due to the fact that the composite layers are mutually parallel and not separated. AFM images of the $MV^{2+}$-$K_4Nb_6O_{17}$ hybrid and the $Ru(bpy)_3^{2+}$-$K_4Nb_6O_{17}$ hybrid are seen in Figure 6.

The surface morphology of the thin film is similar to that seen in the SEM image. The important information obtained from the AFM was the height image, which indicates the basal spacing of the hybrids. The height difference between the two sheets corresponds well to the X-ray diffraction data.

Figure 7 shows the UV spectra of $Ru(bpy)_3^{2+}$ in an aqueous solution (dashed line) and in the interlayer of the $K_4Nb_6O_{17}$ thin film (solid line). The thin film has a sufficient optical

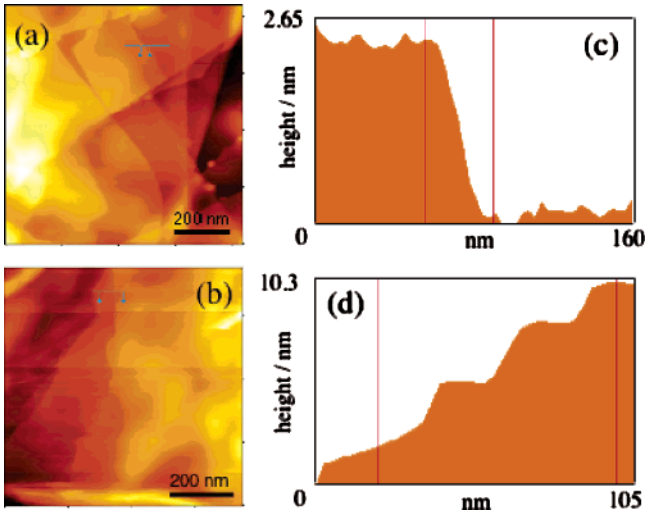


**Figure 6.** AFM images showing the surface morphology of (a) the $MV^{2+}$-$K_4Nb_6O_{17}$ thin film and (b) the $Ru(bpy)_3^{2+}$-$K_4Nb_6O_{17}$ thin film. AFM height images of (c) the $MV^{2+}$-$K_4Nb_6O_{17}$ thin film and (d) the $Ru(bpy)_3^{2+}$-$K_4Nb_6O_{17}$ thin film.

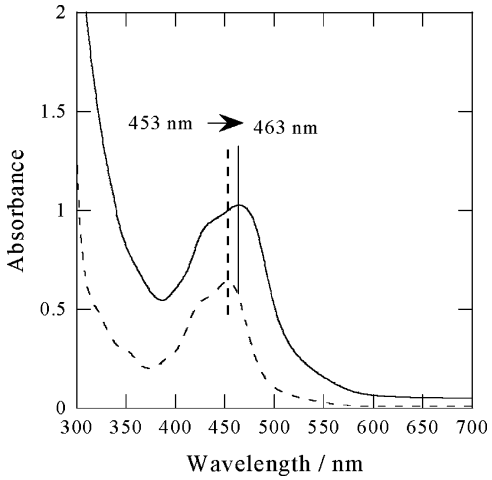


**Figure 7.** Absorption spectrum of $Ru(bpy)_3^{2+}$ in aqueous (dashed line) and $Ru(bpy)_3^{2+}$ intercalation into layered niobate $K_4Nb_6O_{17}$ thin film (solid line).

transparency in the visible region. The $Ru(bpy)_3^{2+}$-$K_4Nb_6O_{17}$ hybrid thin film clearly shows the metal−ligand charge transfer (MLCT) band of $Ru(bpy)_3^{2+}$ with a spectral shape very similar to that of $Ru(bpy)_3^{2+}$ in aqueous solution, except for a 10-nm red shift of the band position. The red shift of the band position for the $Ru(bpy)_3^{2+}$-$K_4Nb_6O_{17}$ hybrid thin film may reflect the microenvironment surrounding $Ru(bpy)_3^{2+}$.[29,37]

The exchange of the $MV^{2+}$ ions by the $Ru(bpy)_3^{2+}$ ions was also supported by infrared spectroscopic analysis, as shown in Figure 8. The IR spectra of the $Ru(bpy)_3^{2+}$-$K_4Nb_6O_{17}$ hybrid exhibited none of the $MV^{2+}$-related absorption bands observed in the $MV^{2+}$-$K_4Nb_6O_{17}$ intercalation compound: The peaks at 2962, 2873 ($\upsilon_{as}$ $CH_3$ and $\upsilon_s$ $CH_3$), 1640 and 1561 (pyridine ring), and 1083 [($\upsilon$ C−N)][38] disappeared, while 1601, 1463, 1442, and 1420 $cm^{-1}$ absorption bands due to the ring-stretching modes for $Ru(bpy)_3^{2+}$ were observed (Figure 8).[39]

On the basis of the observed C, H, and N distribution of 6.54%, 0.68%, and 1.54% for the $Ru(bpy)_3^{2+}$-$K_4Nb_6O_{17}$ hybrid, the composition formula for the $Ru(bpy)_3^{2+}$-$K_4Nb_6O_{17}$ hybrid was calculated to be $(Ru(bpy)_3^{2+})_{0.2}K_{3.6}Nb_6O_{17}\cdot 1.3H_2O$, in which the calculated C/N molar ratio, 4.95 (6.54/12:1.54/14 = 4.95), is in good agreement with the observed value, 5.00. These results indicate that the $MV^{2+}$ ions are completely removed from

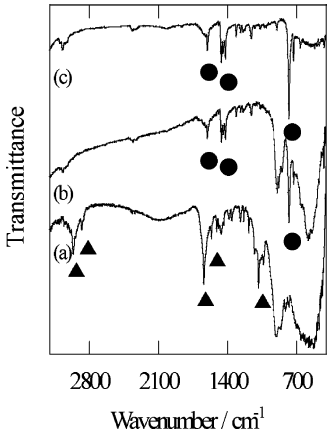


**Figure 8.** Infrared spectra of (a) the $MV^{2+}$-$K_4Nb_6O_{17}$ intercalation compound, (b) the $Ru(bpy)_3^{2+}$-$K_4Nb_6O_{17}$ intercalation compound, and (c) the $Ru(bpy)_3^{2+}Cl_2$ in KBr. The closed triangles indicate the characteristic peaks of $MV^{2+}$, while the closed circles indicate those of $Ru(bpy)_3^{2+}$.

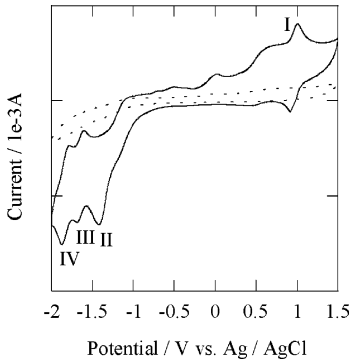


**Figure 9.** Cyclic voltammograms in $CH_3CN$, 0.1 M $Bu_4NBF_4$ for $Ru(bpy)_3^{2+}$ intercalation into layered niobate $K_4Nb_6O_{17}$ thin film on ITO (2 $cm^2$) (solid line) and before intercalation (dashe line). Scan rate, 30 mV/s.

**TABLE 2: Peak Potentials ($E_p$) for Oxidation (I) and Reduction (II−IV) of $Ru(bpy)_3^{2+}$ Intercalation into Layered Niobate $K_4Nb_6O_{17}$ Thin Film**[a]

| | I | II | III | IV |
|---|---|---|---|---|
| $E_{pc}$ (reduction) | +0.921 | −1.413 | −1.683 | −1.876 |
| $E_{pa}$ (oxidation) | +1.006 | −1.115 | -1.606 | −1.791 |
| nb | 1 | 1 | 1 | 1 |

[a] In vs. Ag/AgCl reference electrode. [b] Number of electrons involved in electron-transfer step.

the $Ru(bpy)_3^{2+}$-$K_4Nb_6O_{17}$ hybrid during the guest−guest exchange procedure.

**Electrochemical Measurements with ITO/$Ru(bpy)_3^{2+}$-$K_4Nb_6O_{17}$ Hybrid Thin Film Electrodes.** The cyclic voltammogram (CV) for $Ru(bpy)_3^{2+}$ intercalated into the layered niobate $K_4Nb_6O_{17}$ thin film on an ITO electrode is shown in Figure 9. The background current of the layered niobate $K_4Nb_6O_{17}$ thin film without $Ru(bpy)_3^{2+}$ on ITO is shown as the dashed line. The typical current−potential curve for $Ru(bpy)_3^{2+}$ intercalation into the layered niobate $K_4Nb_6O_{17}$ thin film on ITO is shown as a solid line. The shape of the waves is very different from that expected for a surface-confined species (i.e., symmetrical narrow peaks and anodic and cathode peak separation, $\Delta E_p$, being near zero).[40,41] Instead, the waves have more diffusive tails. The $\Delta E_p$ was 85 mV (at a sweep rate of 30 mV $s^{-1}$), which is significantly larger than the ~59 mV found for $Ru(bpy)_3^{2+}$ oxidation in solution.

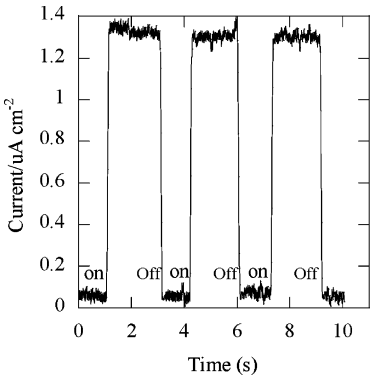


**Figure 10.** Photocurrent response of the ITO/$Ru(bpy)_3^{2+}$-$K_4Nb_6O_{17}$ thin film electrod. Excitation wavelength, 450 nm; electrolyte, 2.5 mM KI in acetonitrile.

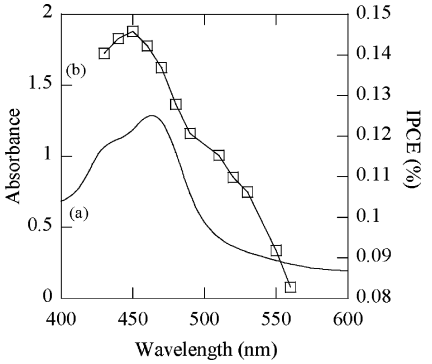


**Figure 11.** (a) Absorption spectrum and (b) action spectrum of the ITO/$Ru(bpy)_3^{2+}$-$K_4Nb_6O_{17}$ electrod (electrolyte, 2.5 mM KI in acetonitrile).

A large $\Delta E_p$ value usually indicates slow heterogeneous electron transfer.[42] Potentials for the oxidation and reduction of $Ru(bpy)_3^{2+}$ intercalated into the layered niobate $K_4Nb_6O_{17}$ thin films are listed in Table 2. All waves represent one-electron transfers. The voltammetric pattern is characterized, in the positive scan, by one reversible oxidation process (peak system I) and three consecutive reduction steps (peaks II, III, and IV) in the negative scan (eqs 1−4).[43]

$$[Ru(bpy)_3]^{2+} \rightleftharpoons [Ru(bpy)_3]^{3+} + e^- \quad \text{(peak I)} \quad (1)$$

$$[Ru(bpy)_3]^{2+} + e^- \rightleftharpoons [Ru(bpy)_3]^{+} \quad \text{(peak II)} \quad (2)$$

$$[Ru(bpy)_3]^{+} + e^- \rightleftharpoons [Ru(bpy)_3]^{0} \quad \text{(peak III)} \quad (3)$$

$$[Ru(bpy)_3]^{0} + e^- \rightleftharpoons [Ru(bpy)_3]^{-} \quad \text{(peak IV)} \quad (4)$$

**Photocurrent Measurements with the ITO/$Ru(bpy)_3^{2+}$-$K_4Nb_6O_{17}$ Hybrid Thin Film Electrode.** As a potential application of the $Ru(bpy)_3^{2+}$-$K_4Nb_6O_{17}$ hybrid thin film, the light energy conversion process using the $Ru(bpy)_3^{2+}$-$K_4Nb_6O_{17}$ hybrid thin film was investigated. Photocurrent generation was observed under visible-light irradiation of the ITO/$Ru(bpy)_3^{2+}$-$K_4Nb_6O_{17}$ hybrid thin film electrode in the presence of $I^-$ as a sacrificial electron donor in the solution phase. An immediate anodic photocurrent response was obtained when the irradiation of the ITO/$Ru(bpy)_3^{2+}$-$K_4Nb_6O_{17}$ hybrid thin film electrode was switched on and off (Figure 10). The photocurrent generation is reproducible under several on/off cycles of irradiation. The photocurrent stability is extremely good in the presence of a sacrificial donor in the electrolyte solution. The photocurrent action spectrum of the ITO/$Ru(bpy)_3^{2+}$-$K_4Nb_6O_{17}$ hybrid thin

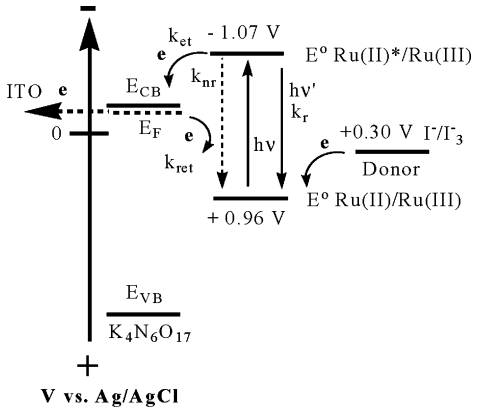


**Figure 12.** Energy level diagram illustrating the conduction (CB) and valence (VB) band energies of $K_4Nb_6O_{17}$ and the oxidation potential ($E°$) of the ground and the excited state of Ru(II). $k_r$, $k_{nr}$, $k_{et}$, and $k_{ret}$ represent rate constants for radiative, nonradiative, charge injection, and reverse electron-transfer processes, respectively.

film electrode is shown in Figure 11. Clearly, $Ru(bpy)_3^{2+}$ is responsible for the photocurrent.

**Mechanism of Photocurrent Generation.** As a mechanism for the anodic photocurrent generation, we propose the following processes (eqs 5−8).

$$ITO/Ru(bpy)_3^{2+}\text{-}K_4Nb_6O_{17} + h\nu \rightarrow ITO/Ru(bpy)_3^{2+}*\text{-}K_4Nb_6O_{17} \quad (5)$$

$$ITO/Ru(bpy)_3^{2+}*\text{-}K_4Nb_6O_{17} \rightarrow ITO/Ru(bpy)_3^{2+}\text{-}K_4Nb_6O_{17} + h\nu \quad (6)$$

$$ITO/Ru(bpy)_3^{2+}*\text{-}K_4Nb_6O_{17} \rightarrow ITO/Ru(bpy)_3^{3+}\text{-}K_4Nb_6O_{17}(e^-) \quad (7)$$

$$2ITO/Ru(bpy)_3^{3+}\text{-}K_4Nb_6O_{17} \xrightarrow[3I^-]{} 2ITO/Ru(bpy)_3^{2+}\text{-}K_4Nb_6O_{17} + I_3^- \quad (8)$$

First, the $Ru(bpy)_3^{2+}$ chromophore is excited by visible light, and then the electron transfer from the excited state to the $K_4Nb_6O_{17}$ conduction band is facilitated. The oxidized $Ru(bpy)_3^{3+}$ accepts an electron from the iodide ion to generate the sensitizer. The electrons transferred to the semiconducting layered niobate sheets are collected at the ITO surface, competing with the back electron transfer to the oxidized $Ru(bpy)_3^{3+}$ within the interlayer, and are driven to the counter electrode through an external circuit to regenerate the redox couple. The scheme illustrated in Figure 12 summarizes the photocurrent at an $ITO/Ru(bpy)_3^{2+}\text{-}K_4Nb_6O_{17}$ electrode.

The values of photon-to-photocurrent conversion efficiency (IPCE) were evaluated from the short-circuit photocurrent measurements at different excitation wavelengths. The IPCE was obtained from the photocurrents by means of the following equation: $IPCE\ (\%) = (1240/\lambda)(I_{sc}/I_{inc}) \sim 100$, where $I_{sc}$ is the short-circuit photocurrent ($A/cm^2$), $I_{inc}$ is the incident light intensity ($W\ cm^{-2}$), and $\lambda$ is the excitation wavelength (nm). The $ITO/Ru(bpy)_3^{2+}\text{-}K_4Nb_6O_{17}$ hybrid thin film electrode shows excellent photoresponse in the visible region. The close match between the photocurrent action spectrum and the absorption spectrum shows that the photosensitization mechanism is operative in extending the photocurrent response of the $ITO/Ru(bpy)_3^{2+}\text{-}K_4Nb_6O_{17}$ hybrid thin film electrode into the visible region. Ruthenium complex having carboxyl groups was reported to adsorb on $SnO_2$,[45] while $Ru(bpy)_3^{2+}$ without the substituents examined here was not adsorbed on ITO at all without niobate and no photocurrent was observed. The photocurrent is, thus, obviously ascribable to the $Ru(bpy)_3^{2+}\text{-}K_4Nb_6O_{17}$ hybrid thin film on ITO. However, the IPCE values are much smaller than the values obtained for $TiO_2$ and $SnO_2$ particulate films with ruthenium complex sensitizers.[44,45] One reason might be the low intrinsic conductivity between the layers. Even when the charge is effectively injected from the excited $Ru(bpy)_3^{2+}$ into the $[Nb_6O_{17}]^{4-}$ sheets with the low interlayer conductivity, charge recombination is favored at each layer over electron transport from the niobate sheets to the ITO electrode. New approaches to improve the interlayer conductivity are required, and this study is now in progress.

## Conclusion

The optically transparent $ITO/Ru(bpy)_3^{2+}\text{-}K_4Nb_6O_{17}$ hybrid thin film electrode was successfully prepared by a guest−guest ion exchange method under ambient conditions. The photosensitizer was successfully and selectively intercalated into only layer I of the optically transparent nanolayered niobate. The optical transparency of the film was excellent as shown (Figure 4). The cyclic voltammogram for $Ru(bpy)_3^{2+}$ intercalated into a layered niobate $K_4Nb_6O_{17}$ thin film on an ITO electrode exhibited a typical current−potential curve for $Ru(bpy)_3^{2+}$ ions. The $ITO/Ru(bpy)_3^{2+}\text{-}K_4Nb_6O_{17}$ hybrid thin film electrode showed an immediate photoresponse in the visible region. The anodic photocurrent generation confirms the charge injection from excited $Ru(bpy)_3^{2+}$ into the semiconductor layered $[Nb_6O_{17}]^{4-}$ sheets. The low IPCE is ascribable to the low intrinsic conductivity between the layers of the $[Nb_6O_{17}]^{4-}$ sheets.

**Acknowledgment.** This work was supported by a grant-in-aid for Scientific Research from Japan Society for the Promotion of Science (JSPS) and the CREST program of the Japan Science and Technology Agency (JST).

## References and Notes

(1) Gasperin, M.; Le Bihan, M. T. *J. Solid State Chem.* **1980**, *33*, 83.
(2) Tong, Z.; Shichi, T.; Kasuga, Y.; Takagi, K. *Chem. Lett.* **2002**, 1206.
(3) Nakato, T.; Kusunoki, K.; Yoshizawa, K.; Kuroda, K.; Kaneko, M. *J. Phys. Chem.* **1995**, *99*, 17896.
(4) Yao, K.; Nishimura, S.; Ma, T.; Okamoto, K.; Inoue, K.; Abe, E.; Tateyama, H.; Yamagishi, A. *J. Electroanal. Chem.* **2001**, *510*, 144.
(5) Sayama, K.; Tanaka, A.; Domen, K.; Maruya, K.; Onishi, T. *J. Phys. Chem.* **1991**, *95*, 1345.
(6) Tawkaew, S.; Yin, S.; Sato, T. *Int. J. Inorg. Mater.* **2001**, *3*, 855.
(7) Ikeda, S.; Tanaka, A.; Shinohara, K.; Hara, M.; Kondo, J. N.; Maruya, K.; Domen, K. *Microporous Mater.* **1997**, *9*, 253.
(8) Koinuma, M.; Seki, H.; Matsumoto, Y. *J. Electroanal. Chem.* **2002**, *531*, 81.
(9) Kinomura, N.; Kumada, N.; Muto. F. *J. Chem. Soc., Dalton Trans.* **1985**, 2349.
(10) Constantino, V. R. L.; Bizeto, M. A.; Brito, H. F. *J. Alloys Compd.* **1998**, *278*, 142.
(11) Ogawa, M.; Kuroda, K. *Chem. Rev.* **1995**, *95*, 399.
(12) Abe, R.; Shinohara, K.; Tanaka, A.; Hara, M.; Kondo, J. N.; Domen, K. *Chem. Mater.* **1998**, *10*, 329.
(13) *Photochemistry on Solid Surface*; Anpo, M., Matsuura, T., Eds.; Studies in Surface Science and Catalysis No. 47; Elsevier: Amsterdam, The Netherlands, 1989.
(14) O'Regan, B.; Grätzel, M. *Nature.***1991**, *353*, 737.
(15) Nazeeruddin, M. K.; Kay, A.; Rodicio, I.; Humphry, B. R.; Mueller, E.; Liska, P.; Vlachopoulos, N.; Grätzel, M. *J. Am. Chem. Soc.* **1993**, *115*, 6382.
(16) Hasobe, T.; Imahori, H.; Fukuzumi, S.; Kamat, P. V. *J. Mater. Chem.* **2003**, *13*, 2515.
(17) Bedja, I.; Hotchandani, S.; Kamat, P. V. *J. Phys. Chem.* **1994**, *98*, 4133.

(18) Barazzouk, S.; Lee, H.; Hotchandani, S.; Kamat, P. V. *J. Phys. Chem. B* **2000**, *104*, 3616.

(19) Nasr, C.; Hotchandani, S.; Kamat, P. V.; Das, S.; George Thomas, K.; George, M. V. *Langmuir* **1995**, *11*, 1777.

(20) Tachibana, Y.; Haque, S. A.; Mercer, I. P.; Durrant, J. R.; Klug, D. R. *J. Phys. Chem. B* **2000**, *104*, 1198.

(21) Tong, Z.; Shichi, T.; Takagi, K. *J. Phys. Chem. B* **2002**, *106*, 13306.

(22) Nazeeruddin, Md. K.; Péchy, P.; Renouard, T.; Zakeeruddin, S. M.; Humphry-Baker, R.; Comte, P.; Liska, P.; Cevey, L.; Costa, E.; Shklover, V.; Spiccia, L.; Deacon, G. B.; Bignozzi, C. A.; Grätzel, M. *J. Am. Chem. Soc.* **2001**, *123*, 1613.

(23) Nazeeruddin, Md. K.; Muller, E.; Humphry-Baker, R.; Vlachopoulos, N.; Grätzel, M. *J. Chem. Soc., Dalton Trans*. **1997**, 4571.

(24) Hotchandani, S.; Kamat, P. V. *Chem. Phys. Lett.* **1992**, *191*, 320.

(25) Ferrrere, S.; Gregg, B. A. *J. Am. Chem. Soc.* **1998**, *120*, 843.

(26) Hagfeldt, A.; Grätzel, M. *Chem. Rev.* **1995**, *95*, 49.

(27) Tennakone, K.; Kumara, G. R. R. A.; Kottegoda, I. R. M.; Perera, V. P. S. *Chem. Commun.* **1999**, 15.

(28) Nakato, T.; Sakamoto, D.; Kuroda, K.; Kato, C. *Bull. Chem. Soc. Jpn.* 1**992**, *65*, 322.

(29) Yao, K.; Nishimura, S.; Imai, Y.; Wang, H.; Ma, T.; Abe, E.; Tateyama, H.; Yamagishi, A. *Langmuir* **2003**, *19*, 321.

(30) Furube, A.; Shiozawa, T.; Ishikawa, A.; Wada, A.; Domen, K.; Hirose, C. *J. Phys. Chem. B* **2002**, *106*, 3065.

(31) Abe, R.; Ikeda, S.; Kondo, J. N.; Hara, M.; Domen, K. *Thin Solid Films* **1999**, *343−344*, 156.

(32) Nassau, K.; Shiever, W.; Bernstein, J. L. *J. Electrochem. Soc.* **1969**, *116*, 348.

(33) Nakato, T.; Kuroda, K.; Kato, C. *Catal. Today* **1993**, *16*, 471.

(34) Nakato, T.; Kuroda, K.; Kato, C. *J. Chem. Soc., Chem. Commun.* **1989**, 1144.

(35) Raupach, M.; Emerson, W. W.; Slade, P. G. *J. Colloid Interface Sci.* **1979**, *69*, 398.

(36) Poizat, O.; Sourisseau, C.; Mathey, M. M. *J. Chem. Soc., Faraday Trans. 1* **1984**, *80*, 3257.

(37) Krenske, D.; Abdo, S.; Van Damme, H.; Cruz, M.; Fripiat, J. J. *J. Phys. Chem.* **1980**, *84*, 2447.

(38) Miyata, H.; Sugahara, Y.; Kuroda, K.; Kato, C. *J. Chem. Soc., Faraday Trans. 1* **1988**, *84*, 2677.

(39) Poizat, O.; Sourisseau, C. *J. Phys. Chem.* **1984**, *88*, 3007.

(40) Merz, A.; Bard, A. J. *J. Am. Chem. Soc.* **1978**, *100*, 3223.

(41) Lexa, D.; Savéant, J. M. *J. Am. Chem. Soc.* **1978**, *100*, 3222.

(42) Rubinstein, I.; Bard, A. J. *J. Am. Chem. Soc.* **1981**, *103*, 5007.

(43) Richter, M. M.; Bard, A. J. *Anal. Chem.* **1998**, *70*, 310.

(44) Nazeeruddin, M. K.; Kay, A.; Rodicio, I.; Humphry-Baker, R.; Müller, E.; Liska, P.; Vlachopoulos, N.; Grätzel, M. *J. Am. Chem. Soc.* **1993**, *115*, 6382.

(45) Kamat, P. V.; Bedja, I.; Hotchandani, S.; Patterson, L. K. *J. Phys. Chem.* **1996**, *100*, 4900.